

Gear tooth pitting modelling and detection based on transmission error measurements

Nabih Feki*, Jérôme Cavoret, Fabrice Ville and Philippe Vexex

*LaMCoS, INSA Lyon, Université de Lyon, UMR CNRS 5259, Bâtiment Jean d'Alembert 20,
Avenue Albert Einstein, Villeurbanne Cedex 69621, France*

In this study, an experimental validation of a 3D gear dynamic model in the presence of localised faults such as pitting on tooth flanks is proposed. The corresponding numerical model accounts for spur and helical gear systems including gear errors and deviations along with the supporting shafts and bearings. Simulation results are compared with the evidence from a back-to-back test rig and the model validation relies on loaded transmission error (TE) measurements. Many numerical and experimental results on dynamic behaviours due to the presence of tooth pitting in geared systems are presented. Based on TE measurements, it is demonstrated that the actual vibrations generated by gear tooth pitting validate the gear model and its extension to consider such tooth surface failures.

Keywords: gear; transmission error; tooth pitting; diagnosis; modelling

1. Introduction

Geared transmission systems are frequently integrated in many industrial applications because of their reduced cost, power-to-weight ratio and high degree of reliability. Because of the critical role of gears in these systems, gear failures diagnosis and monitoring are required for optimal and/or preventive maintenance especially for high power applications in order to reduce technical and financial losses.

In this context, the dynamic behaviour of geared systems has been widely studied over the last 30 years initially based on linear models neglecting the non-linear contribution of contact conditions such as possible contact losses during motion and, progressively, more sophisticated non-linear dynamic models with variable mesh stiffness adapted to the simulations of actual dynamic behaviour including the influence of geometrical errors and assembly defects. Transmission error (TE) under load at low speed is classically defined as the difference between the actual and theoretical gear angular positions and it is widely accepted as a reliable indicator of the vibration and noise performance of narrow-faced gears (Vexex & Ajmi, 2006).

In this study, a numerical three-dimensional gear model is presented which makes it possible to simulate the non-linear dynamic behaviour of a spur or helical gears, shafts and bearings. The pinion and the gear bodies are assimilated to rigid-cylinders connected by a series of time-varying, non-linear springs representing the mesh stiffness function (Vexex & Maatar, 1996). Gear tooth faults such as pitting can be introduced

*Corresponding author. Email: Nabih.Feki@insa-lyon.fr

anywhere on the active tooth flanks by some suitable localized distributions of normal initial separations with respect to the errorless tooth flanks (Feki, Clerc, & Velex, 2012). The shafts are simulated by two-node classic elements, whereas the bearings are accounted for by additional lumped stiffness elements. On the other hand, experimental investigations were conducted using a standard power circulating Forschungsstelle für Zahnräder und Getriebbau (FZG) fatigue test rig in order to generate real pitting failures on tooth flanks. The test rig was instrumented by optical encoders to continuously measure TEs under load and appraise the influence of pits on mesh excitations.

The study is organized as follows. The first section is dedicated to the description of the numerical gear dynamic model with pitting failures on gear teeth followed by the description of the experimental set-up along with the measurement principles and methodology. Then, based on TE spectral analyses, it is shown that the frequencies associated with the defects can be easily identified. The experimental and simulated results agree fairly well, thus validating the gear dynamic model and its extension to implementing a tooth pitting model.

2. 3D dynamic gear model

2.1. Gear model description

The model, described in Figure 1(a), is composed of five basic elements: (1) the input and output shafts simulated by two-node Timoshenko beam elements with circular cross sections, (2) the pinion-gear pair assimilated to two rigid-cylinders linked by a series of time-varying, non-linear springs accounting for the time-variations of mesh stiffness and contact non-linearity (Velex & Maatar, 1996), (3) the bearings introduced as additional lumped stiffness elements (Abousleiman & Velex, 2006), (4) a motor and a load machine imposing, respectively, the input torque at the first node of the pinion shaft and the resisting load at one node of the gear shaft (output). The total model comprises six nodes with six degrees-of-freedom (DOFs) per node corresponding to the infinitesimal generalized elastic displacements superimposed on rigid-body motions (Raclot & Velex, 1999). The pinion-gear pair DOFs are shown in Figure 1(b).

2.2. Contact simulation

Following Velex and Maatar (1996), mesh elasticity is modelled by a distribution of independent stiffness elements along the theoretical contact lines in the base plane (Wrinkler foundation) as illustrated in Figure 2. The base plane is one of the tangent planes to both the pinion and gear base cylinders (Figure 1(b)), where all the contacts between the teeth take place for involute tooth profiles. Each stiffness element $k(M_{ij})$ associated with any potential point of contact M_{ij} is time and position dependent as the relative positions of the meshing teeth vary during the gear rotation (Figure 2). The stiffness functions have been determined by using the classic results of Weber and Banascheck (1953) for tooth bending and base displacements (every tooth is assimilated to a variable thickness cantilever fixed to an elastic half-plane). The non-linear formula of Lundberg (1939) is employed for contact deflections assuming that pressure distributions are semi-elliptical in the profile direction and constant across the contact line. All the displacements described above are then superimposed and the (tangent) stiffness is deduced by differentiating the force with respect to the total displacement.

Figure 2 shows an instantaneous configuration of the contact between pinion and gear profiles in the base plan in the case of helical gears (β_b : helix angle). The contact

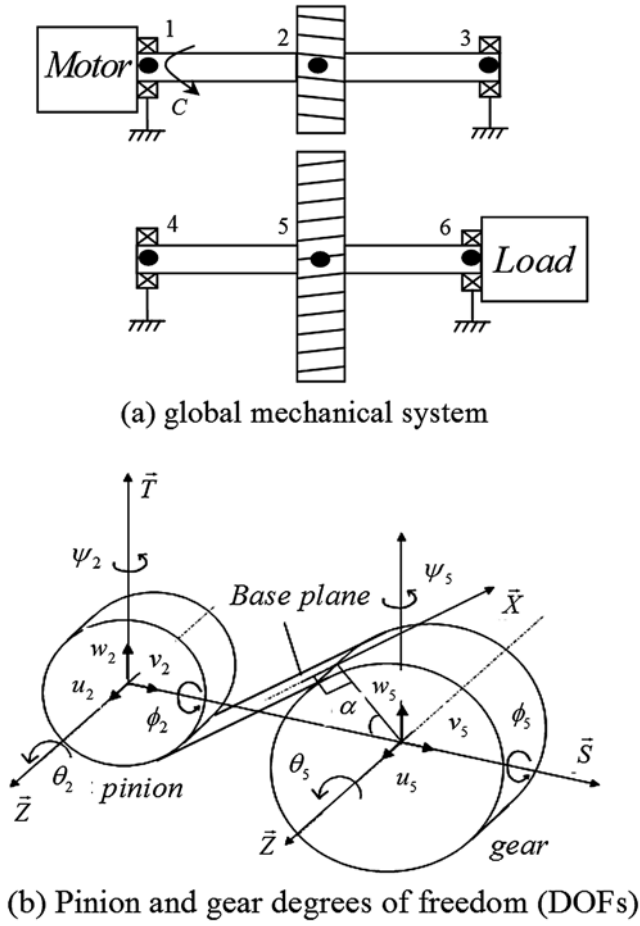


Figure 1. 3D dynamic gear model (36 DOFs).

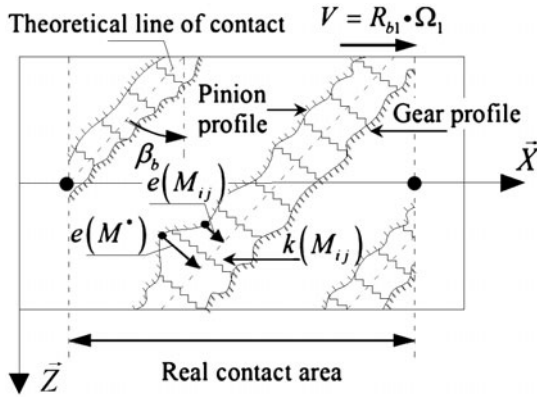


Figure 2. Mesh stiffness modelling in the base plane.

lines evolve over time in the real contact area with respect to the speed V . Each contact line is discretised into several segments and at each segment, an elemental mesh stiffness $k(M_{ij})$ and an equivalent error $e(M_{ij})$ are associated (cell ij : segment j of contact line i). $e(M^*)$ is the maximum of equivalent errors $e(M_{ij})$ in the base plane. The instantaneous contact line positions in the base plane are determined and updated based on rigid-body rotations in order to simulate the meshing process and, at every time step, the actual elemental mesh stiffness are re-calculated.

2.3. Tooth pitting model

From a simulation point of view, every localized fault such as a tooth pit or spall is assimilated to a distribution of initial separations $e(M_{ij})$ (Figure 2) with respect to ideal tooth shapes (El Badaoui, Cahouet, Guillet, Danière, & Velez, 2001) at some points on the flanks (transposed on the base plane). As illustrated in Figure 3, the resulting tooth error functions are three-dimensional and depend on: (a) the varying defect width in the contact line direction (tooth face width), (b) its extent in the profile direction (tooth height), and (c) its varying depth distribution which is simulated by using Bezier's function $B_e(t)$ (Figures 3 and 4) in order to introduce realistic spall morphologies (Olver, 2005) and avoid discontinuities, when tooth faults come into the contact zone. The shape deviations associated with spalls are approximated as $e(M_{ij}) = \Pi_{ij} \cdot B_e(t)$, Where Π_{ij} is a windowing function, which is equal to 1 within the fault area on the base plane and zero outside the defect area (Figure 4).

The deflection at any potential point of contact M_{ij} on the tooth flanks can be expressed as follows:

$$\Delta(M_{ij}) = \mathbf{V}(\mathbf{M}_{ij})^T \mathbf{q} - \delta e(M_{ij}) \quad (1)$$

where $\mathbf{q} = \{v_2, w_2, u_2, \varphi_2, \psi_2, \theta_2, v_5, w_5, u_5, \varphi_5, \psi_5, \theta_5\}^T$ is the pinion-gear pair DOF vector (Figure 1(b)); $\delta e(M_{ij}) = e(M_{ij}) - e(M^*)$ represents the equivalent normal deviation at point M_{ij} with respect to ideal flanks (theoretical contact lines (Figure 2)) and accounts for geometrical errors produced by spalls, ... etc.; $e(M^*)$ is the maximum of

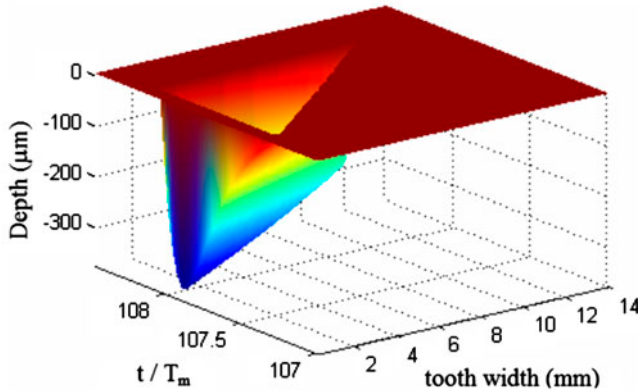


Figure 3. Gear pit form and dimensions.

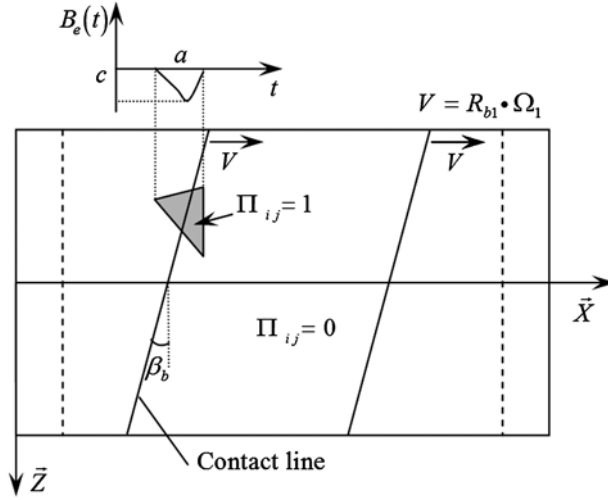


Figure 4. Simulation of the contact line passage within the spall surface on the base plane.

$e(M_{ij})$ at every time step; $\mathbf{V}(M_{ij})$ is the pinion-gear structural vector associated with point M_{ij} which embodies the pinion-gear geometrical proprieties at M_{ij} and reads:

$$\mathbf{V}(M_{ij}) = \{ \mathbf{n} \quad \mathbf{O}_2 \mathbf{M}_{ij} \times \mathbf{n} \quad -\mathbf{n} \quad -\mathbf{O}_5 \mathbf{M}_{ij} \times \mathbf{n} \}^T \quad (2)$$

where \mathbf{n} is the outward unit normal vector with respect to the pinion flanks.

2.4. Equations of motion

Centrifugal and gyroscopic effects being neglected, the equations of motion point to a non-linear parametrically excited differential system of the form (Feki et al., 2012; Velex & Maatar, 1996):

$$\mathbf{M}\ddot{\mathbf{X}} + \mathbf{C}\dot{\mathbf{X}} + \mathbf{K}(t, \mathbf{X})\mathbf{X} = \mathbf{F}_0(t) + \mathbf{F}_{e1}(t, \mathbf{X}) + \mathbf{F}_{e2}(t) \quad (3)$$

where $\mathbf{X} = \{v_1, w_1, u_1, \varphi_1, \psi_1, \theta_1, v_2, \dots, \theta_5, v_6, w_6, u_6, \varphi_6, \psi_6, \theta_6\}^T$ is the DOF's vector; \mathbf{M} , \mathbf{C} and $\mathbf{K}(t, \mathbf{X})$ are the total mass, viscous damping and time-dependent non-linear stiffness matrices, respectively; $\mathbf{F}_0(t)$ is the nominal torque vector; $\mathbf{F}_{e1}(t, \mathbf{X})$ is an additional excitation vector generated by tooth shape deviations (including pits or spalls); $\mathbf{F}_{e2}(t)$ is an additional inertial vector caused by unsteady rotational speeds (due to gear faults).

The total mass matrix is classic, whereas the global viscous damping matrix is defined via a pseudo-modal basis derived from the system at rest with averaged mesh stiffness (Abousleiman & Velex, 2006). In this study, the damping matrix is determined using a unique modal damping factor of 0.1 for all the retained modes. The time-dependent global stiffness matrix and additional forcing vectors represent the gear mesh elasticity variations caused by the contact length evolutions on tooth flanks, tooth shape deviations and errors (Feki, Clerc, & Velex, 2013), they read as follows:

$$\mathbf{K}(t, \mathbf{X}) = \mathbf{K}_c + \sum_i^{N_l} \sum_j^{N_s} (k(M_{ij})H(\Delta(M_{ij}))\mathbf{V}(\mathbf{M}_{ij})\mathbf{V}(\mathbf{M}_{ij})^T) \quad (4)$$

$$\mathbf{F}_{e1}(t, \mathbf{X}) = \sum_i^{N_l} \sum_j^{N_s} (k(M_{ij})H(\Delta(M_{ij}))\delta e(M_{ij})\mathbf{V}(\mathbf{M}_{ij})) \quad (5)$$

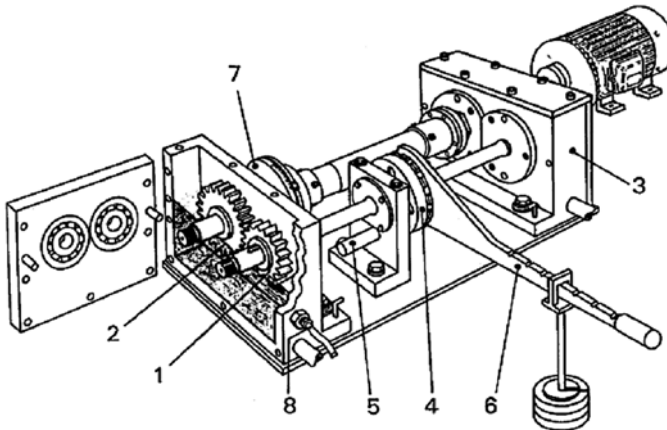
where \mathbf{K}_c is a constant matrix comprising the constant stiffness elements associated with the shaft-bearing assembly; $\mathbf{V}(\mathbf{M}_{ij})$ is the extended gear structural vector (as described in Equation (2)) completed by zeros to the total system size; $k(M_{ij})$ is the elemental stiffness at cell ij : segment j of contact line i (Figure 2); N_l is the number of time-dependent contact lines in the base plane; N_s is the number of time-dependent segments for each contact line in the base plane and finally, $H(\Delta(M_{ij}))$ is the Heaviside unit function which is equal to one when $\Delta(M_{ij}) > 0$ (see Equation (1)) and zero otherwise (i.e. when the contact at point M_{ij} is lost).

The differential system (3) is solved iteratively by combining an implicit Newmark's time-step integration scheme and a unilateral contact algorithm which, at every time-step, verifies that the contact conditions are satisfied (compressive contact forces, no penetration of the parts outside the contact zone) (Velex & Ajmi, 2006).

3. Experimental set-up

3.1. Description of the FZG gear test rig

The FZG gear test rig was originally developed at the FZG of the Technical University of Munich. It is an electromechanical system composed of an asynchronous motor with a speed controller (100–3000 rpm) and a back-to-back rig consisting in test and slave gears connected by two shafts (Figure 5). The secondary shaft is divided in two parts



- | | | |
|---------------|--------------------------|---------------------------|
| 1 Test pinion | 4 Load clutch | 7 Torque measuring clutch |
| 2 Test wheel | 5 Locking pin | 8 Temperature sensor |
| 3 Slave gear | 6 Load lever and weights | |

Figure 5. FZG back-to-back gear test rig (Höhn et al., 2008).

with the load clutch. This device is fixed on one side to the foundation by means of a locking pin. On the other side, the half shaft is twisted using a lever and weights in order to apply a static load. This torsion torque is kept constant during the operation of the test bench after bolting the clutch, removing the weights and lever and unlocking the shaft.

This machine was specifically designed for testing highly-loaded gears and the related fatigue issues (contact and root stresses). High powers can be reached to the power circulation and the capability to impose a torque by elastic deformation independently of the speed imposed by the electrical motor controller.

3.2. Measurement principle

From an experimental point of view, TE can be measured by systems based on accelerometers or high-resolution optical encoders. In the present case, TE was derived from the data of two optical encoders mounted on the free-ends of either shafts of the gear system as illustrated in Figure 6.

The optical encoders were mounted very close to the test pinion and gear in order to make TE measurements as representative as possible of the gear behaviour. The measurement principle relies on counting the number of pulses from a timer signal with a very high frequency (80 MHz here) between two rising edges of the optical encoder signal (Remond, 1998). Having a common reference (same timer and counter), the counting can be simultaneously performed on the two channels. Figure 7(a) shows a simplified scheme leading to the reconstruction of the time variations of the pinion and gear angular positions (De Vaujany, Remond, & Guingand, 2005) in relation to the number of encoder pulses per revolution (here, 2500 pulses).

3.3. Experimental TE calculation

Having stored the measured time lengths between successive rising edges from both encoders, TE can be deduced by using several methods. According to Remond and Play (1999), the so-called “angular methods” seem to be more representative of physical phenomena than asynchronous methods (Remond & Play, 1999). In fact, the use of angular methods leads to bring out the dynamic effects of gear geometry, eccentricity, tooth meshing and especially gear tooth faults. This method consists in sampling the gear angular position with reference to the pinion angular position (Figure 7(b)). Then, the new gear angular position $\theta_2(i)$ is resolved by linear interpolation at times corresponding to the number of timer pulses between two consecutive rising edges of the pinion encoder. The TE formula can then be numerically reconstructed by taking into account the speed ratio leading to an expression of the form:

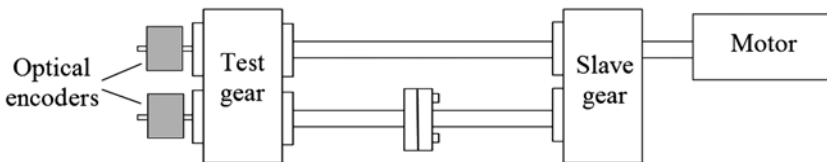


Figure 6. Optical encoders mounting positions on FZG back-to-back gear test rig.

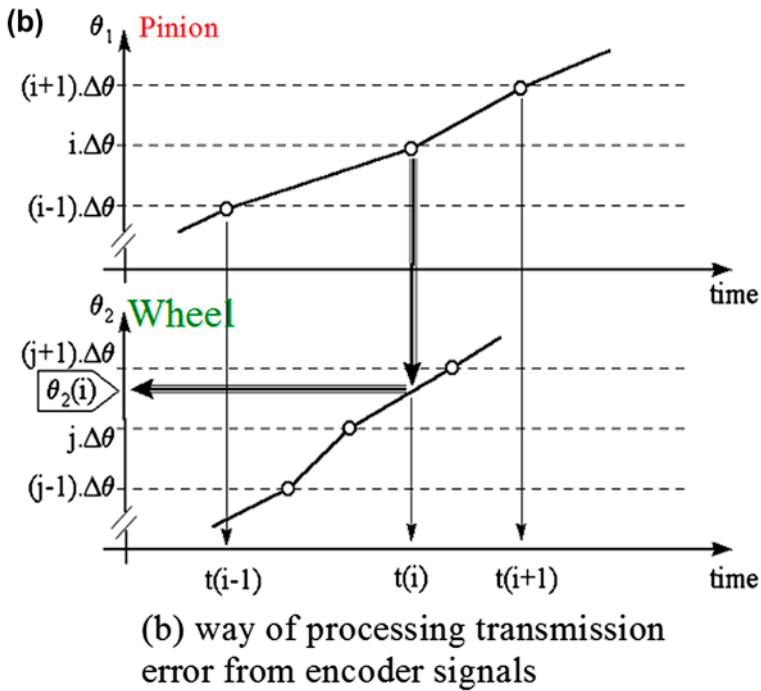
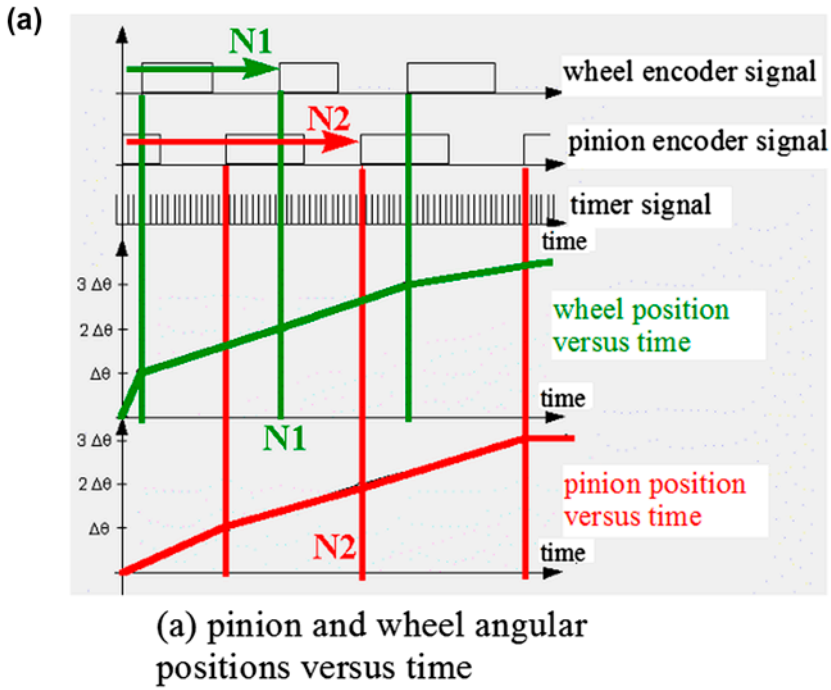


Figure 7. Measurement principle (De Vaujany et al., 2005).

$$TE(i) = \theta_1(i) - \frac{Z_2}{Z_1}\theta_2(i) = i \cdot \Delta\theta_1 - \frac{Z_2}{Z_1}\theta_2(i). \quad (6)$$

4. Results and discussion

All the following results have been obtained for a test spur gear whose characteristics are detailed in Table 1 (Höhn, Oster, Tobie, & Michaelis, 2008).

4.1. Generation of actual pitting

In order to investigate the vibration behaviour of a spur gear in the presence of pitting, a fatigue test was performed to generate “natural” gear tooth pitting. The test conditions, taken from DGMK Information Sheet (2006), are intended to lead to pitting (short duration test pitting). In short, it consists in applying very important loading levels (levels 9 and 10 in Table 2) at a constant rotational speed, while controlling the oil temperature in the gearbox (90 ± 3 °C (DGMK Information Sheet, 2006)). The torque applied to the output shaft causes a force distribution on the tooth contact surfaces resulting in local Hertzian pressure distributions (a maximal local Hertzian contact stress of 2069 N/mm² for loading level 9 (DGMK Information Sheet, 2006)). This type of fatigue test is mainly used to determine the influence of lubricants on pitting resistance.

During fatigue testing, the test gearbox was cooled down in order to be able to run the machine continuously until contact failures appear. A unique spall was detected on one pinion tooth after 13 million cycles which is shown in Figure 8 (C-type gears).

The dimensions of the actual pitting failure on the tooth are given in Figure 9(a) where t/T_m (T_m is the mesh period) represents a dimensionless time but also the normalised position in the profile direction. The defect is characterized by a triangular shape on the tooth surface with a maximum depth around 380 µm. In order to compare the numerical and experimental results, this defect has been simulated as a hole on one pinion tooth whose geometry is close to that of the actual fault as illustrated in Figure 9(b).

4.2. Comparison between measured and simulated TE spectra

Figures 10–13 show the spectra of the experimental and theoretical (simulated) TE signals of the test gear with and without the presence of a pit in one tooth of the pinion. The TE signals have been obtained for a rotational speed of 30 Hz on the input shaft

Table 1. Main geometrical characteristics of test spur gear (C-type).

	Pinion	Gear
Centre distance (mm)	91.5	
Number of teeth	16	24
Module (mm)	4.5	
Pressure angle (°)	20	20
Face width (mm)	14	14
Pitch diameter (mm)	73.2	109.8
Profile shift coefficient	0.1817	0.1715

Table 2. Loading levels.

Loading levels	4	5	6	7	8	9	10
Load torque (Nm)	60.75	94.1	135.3	183.35	239.25	302	372.7
Input torque (Nm)	91.12	141.15	202.95	275.02	358.87	453	559.05

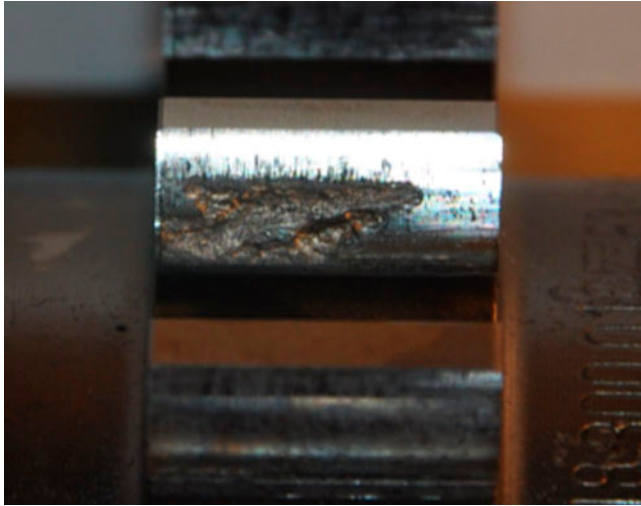


Figure 8. Actual gear tooth pitting.

and under loading level 7 (as defined in Table 2). All the spectra have been calculated using a Blackman window in order to obtain narrow and distinctive peaks and amplitudes have been divided by the maximum amplitude in each case.

For the same operating conditions, it can be noticed that the spectra of the experimental and simulated signals (with or without tooth pitting) look similar. In all the cases, significant amplitude is reported at the fifth harmonic of the mesh frequency. According to the simulation results, this frequency corresponds to a critical frequency of the mechanical system (test gear, shafts and bearing) with a very large contribution of the gear element (84.19%) to the total modal strain energy. In the presence of one tooth pit, the spectra exhibit modulation sidebands between the different gear mesh harmonics mainly around the first and fifth harmonics. However, these sidebands are not present in the TE spectra of healthy gears. For example, between harmonics 4 and 5 or 5 and 6, 16 peaks emerge in the TE spectra with pitting (Figures 11 and 13). These peaks are spaced by integer multiples of the pinion rotational frequency and their number (between two harmonics) corresponds to the pinion tooth number. This explains that, in the presence of a fault, the frequency modulation is controlled by the rotational frequency of the defective wheel (pinion in our case).

It is also noticed that the TE spectra with pitting reveal asymmetric sideband distributions typical of both amplitude and frequency modulations. The main reasons for this asymmetry are, (1) the dynamic effects caused by the vicinity of these sidebands and

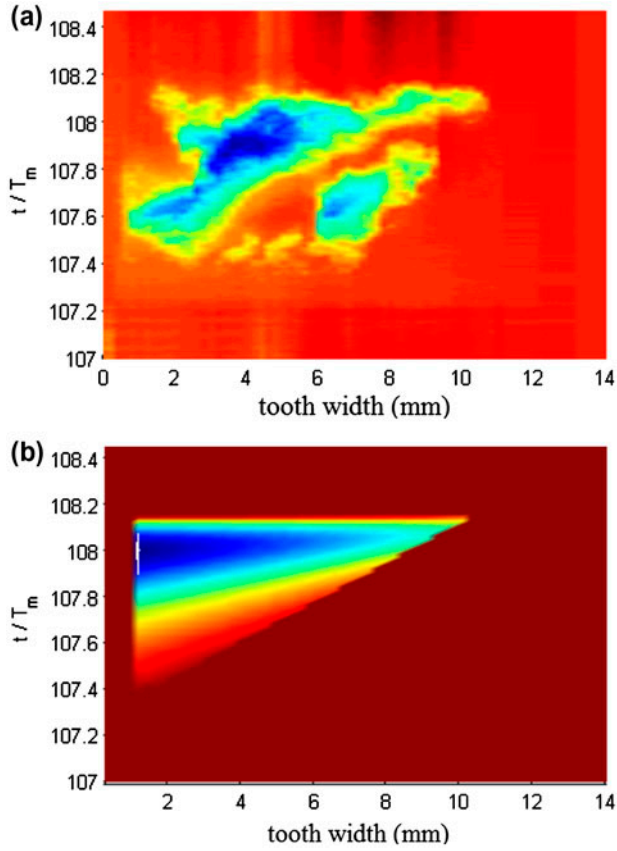


Figure 9. (a) Actual and (b) simulated tooth pitting.

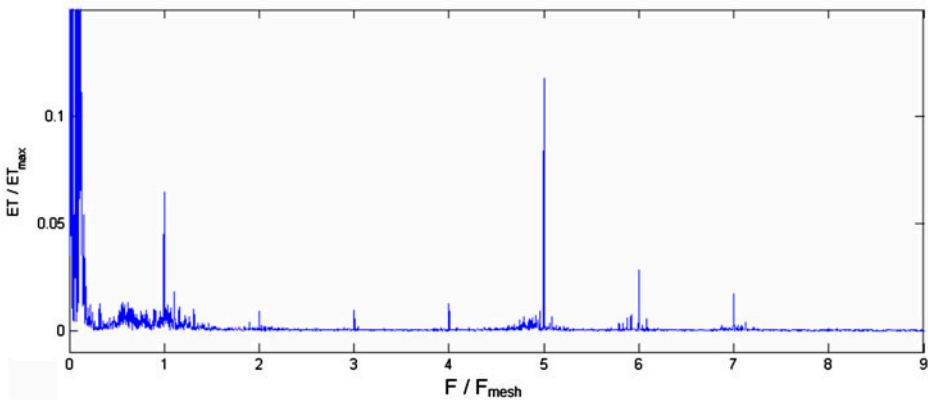


Figure 10. Spectrum of the experimental TE signal without gear tooth pitting.

the resonance zone (critical frequencies) (Inalpolat & Kahraman, 2009; McFadden & Smith, 1985), and (2) the effect of the carrier frequency of the pinion rotation on modulation sidebands (Inalpolat & Kahraman, 2009).

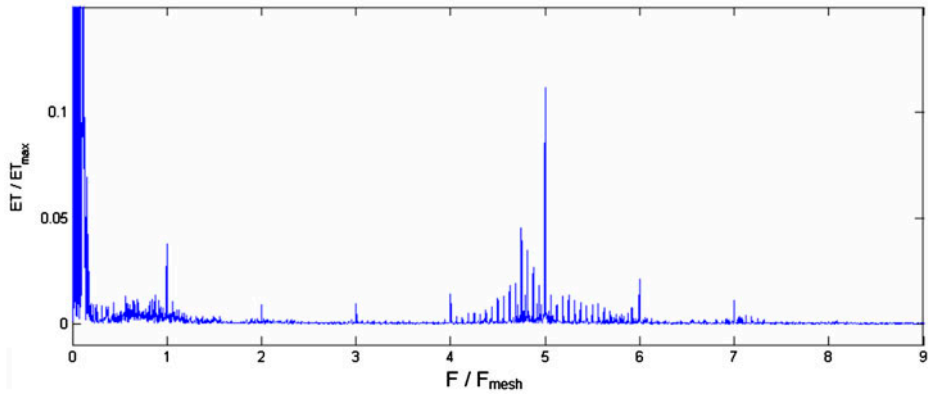


Figure 11. Spectrum of the experimental TE signal in the presence of a tooth pit.

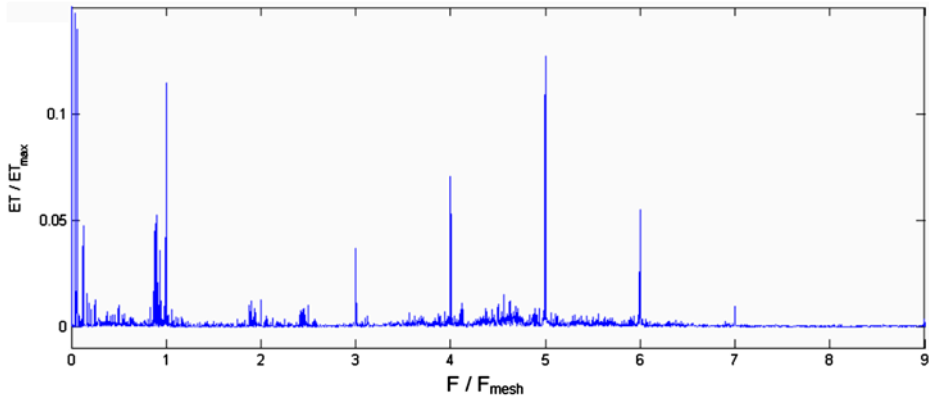


Figure 12. Spectrum of the simulated TE signal without gear tooth pitting.

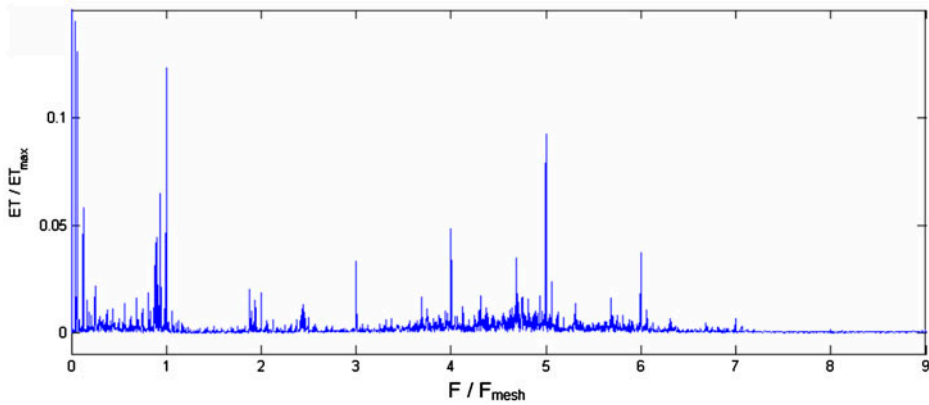


Figure 13. Spectrum of the simulated TE signal in the presence of a tooth pit.

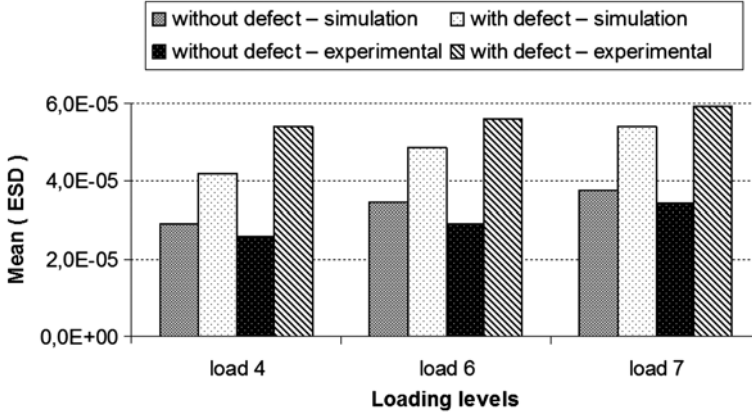


Figure 14. Mean ESD on the frequency band $[4 \cdot F_{\text{mesh}}, 6 \cdot F_{\text{mesh}}]$ of the spectra of experimental and simulates signals, with and without spall, for different loading levels.

4.3. Influence of tooth pitting on the mean energy spectral density

According to Stoica and Moses (2005), the so-called energy spectral density (ESD) characterises the distribution of sequence (signal) energy as a function of frequency. The ESD is particularly suited for the analysis of transients and signals perturbed by faulty elements.

The mean ESD of the TE signal is defined as follows:

$$\text{Mean(ESD)} = \frac{\sum_{i=1}^N (\text{TE}(f_i))^2}{N} \quad (7)$$

where N is the number of peaks over a frequency band and $\text{TE}(f_i)$ is the spectrum amplitude at frequency f_i .

Figure 14 shows the mean ESD over the frequency band $[4 \cdot F_{\text{mesh}}, 6 \cdot F_{\text{mesh}}]$ for the experimental and numerical spectra, with and without spall and various loading levels. It is noted that the presence of one spall on tooth flanks leads to an increase in the mean ESD in the considered frequency band. This phenomenon has been observed for all loading levels and in both the theoretical and experimental TE signals. The presence of a localised fault on one tooth manifests itself by higher peak amplitudes associated with the pinion rotational frequency, which corresponds to the frequency of passage of the defective tooth in the mesh. On the other hand, the mean spectral density energy increases slightly for larger loads for all the signals (with and without spall, theoretical and experimental). It can, therefore, be inferred that the mean ESD can be used for the detection of gear tooth failures. Moreover, the evaluation of the mean over the frequency band including the sidebands around the harmonics of the mesh frequency is very sensitive to transmission effects.

5. Conclusion

A model has been presented which can be used for simulating the contribution of localized tooth faults such as pits on tooth flanks. The simulation results compare favourably with the evidence from a back-to-back test rig instrumented with encoders, thus

validating the proposed modelling strategy. It is also confirmed that TE signals can be employed in order to detect and monitor tooth surface failures. The presence of one tooth fault leads to significant modulation sidebands near the mesh frequency and its harmonics that are spaced by integer multiples of the rotational frequency of the faulty gear. In this context, ESD appears as a reliable and sensitive tool for the early detection by vibration monitoring.

References

- Abousleiman, V., & Velex, P. (2006). A hybrid 3D finite element/lumped parameter model for quasi-static and dynamic analyses of planetary/epicyclic gear sets. *Mechanism and Machine Theory*, *41*, 725–748.
- De Vaujany, J.-P., Remond, D., & Guingand, M. (2005). Numerical simulation and measurement of gear transmission error of aeronautical spiral bevel gears. In *Proceeding of the XVII French Congress of Mechanics*.
- DGMK Information Sheet (2006). Short test procedure to investigate the lubricant influence on the pitting carrying capacity of gears. Deutsche Wissenschaftliche Gesellschaft für Erdöl, Erdgas und Kohle e.V.
- El Badaoui, M., Cahouet, V., Guillet, F., Danière, J., & Velex, P. (2001). Modeling and detection of localized tooth defects in geared systems. *ASME, Journal of Mechanical Design*, *123*, 422–430.
- Feki, N., Clerc, G., & Velex, P. (2012). An integrated electro-mechanical model of motor-gear units – Applications to tooth fault detection by electric measurements. *Mechanical Systems and Signal Processing*, *29*, 377–390.
- Feki, N., Clerc, G., & Velex, P. (2013). Gear and motor fault modeling and detection based on motor current analysis. *Electric Power Systems Research*, *95*, 28–37.
- Höhn, B.-R., Oster, P., Tobie, T., & Michaelis, K. (2008). Test methods for gear lubricants. *Goriva i Maziva*, *47*, 129–152.
- Inalpolat, M., & Kahraman, A. (2009). A theoretical and experimental investigation of modulation sidebands of planetary gear sets. *Journal of Sound and Vibration*, *323*, 677–696.
- Lundberg, G. (1939). Contact of two elastic half-spaces. *Forschung auf dem Gebiete des Ingenieurwesens*, *10*, 201–211.
- McFadden, P. D., & Smith, J. D. (1985). An explanation for the asymmetry of the modulation sidebands about the tooth meshing frequency in epicyclic gear vibration. *Proceedings of the Institution of Mechanical Engineers*, *199*, 65–70.
- Olver, A. V. (2005). The mechanism of rolling contact fatigue: An update. *Journal of Engineering Tribology*, *219*, 313–330.
- Raclot, J.-P., & Velex, P. (1999). Simulation of the dynamic behaviour of single and multi-stage geared systems with shape deviations and mounting errors by using a spectral method. *Journal of Sound and Vibration*, *220*, 861–903.
- Remond, D. (1998). Practical performances of high-speed measurement of gear transmission error or torsional vibrations with optical encoders. *Measurement Science & Technology*, *9*, 347–353.
- Remond, D., & Play, D. (1999). *Advantages and perspectives of gear transmission error measurement with optical encoders*. Paris: Congrès Mondial des Engrenages et Transmissions.
- Stoica, P., & Moses, R. L. (2005). *Spectral analysis of signals*. Upper Saddle River, NJ: Pearson/Prentice Hall.
- Velex, P., & Ajmi, M. (2006). On the modeling of excitations in geared systems by transmission errors. *Journal of Sound and Vibration*, *290*, 882–909.
- Velex, P., & Maatar, M. (1996). A mathematical model for analyzing the influence of shape deviations and mounting errors on gear dynamic behaviour. *Journal of Sound and Vibration*, *191*, 629–660.
- Weber, C., & Banaschek, K. (1953). *Shape change and profile relief for spur and helical gears*. *Schriftenreihe Antriebstechnik*, *11*, Braunschweig: F. Vieweg und Sohn.